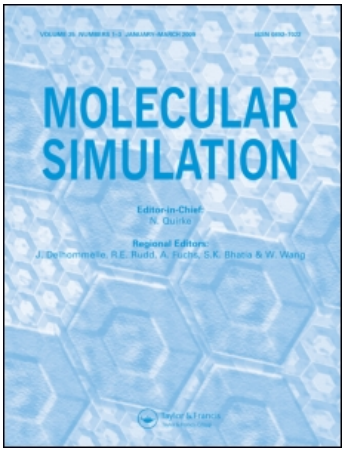

Molecular Simulation
Publication details, including instructions for authors and subscription information:
http://www.informaworld.com/smpp/title~content=t713644482

Industrial Applications of Simulation Studies in Solid State Chemistry

C. R. A. Catlow[a]; P. A. Cox[a]; R. A. Jackson[a]; S. C. Parker[b]; G. D. Price[c]; S. M. Tomlinson[a]; R. Vetrivel[a]
[a] Department of Chemistry, University of Keele, Staffs [b] School of Chemistry, University of Bath, Bath [c] Department of Geological Sciences, University College London, London

To cite this Article Catlow, C. R. A. , Cox, P. A. , Jackson, R. A. , Parker, S. C. , Price, G. D. , Tomlinson, S. M. and Vetrivel, R.(1989) 'Industrial Applications of Simulation Studies in Solid State Chemistry', Molecular Simulation, 3: 1, 49 — 69
To link to this Article: DOI: 10.1080/08927028908034619
URL: http://dx.doi.org/10.1080/08927028908034619

Molecular Simulation, 1989, Vol. 3, pp. 49–69
Reprints available directly from the publisher
Photocopying permitted by license only

INDUSTRIAL APPLICATIONS OF SIMULATION STUDIES IN SOLID STATE CHEMISTRY

C.R.A. CATLOW,* P.A. COX,* R.A. JACKSON,* S.C. PARKER,†, G.D. PRICE‡, S.M. TOMLINSON* and R. VETRIVEL*

**Department of Chemistry, University of Keele, Staffs., ST5 5BG*
†School of Chemistry, University of Bath, Claverton Down, Bath, BA2 7AY
‡Department of Geological Sciences, University College London, Gower St., London WC1E 6BT

(*Received June 1988; in final form August 1988*)

This paper gives an account of some recent applications of computer simulation techniques to materials of industrial importance. The methodology used is fully discussed, and applications to zeolites, high T_c superconductors, superionic conductors and mantle-forming minerals are described.

KEY WORDS: Computer simulation, zeolites, high T_c superconductors, superionic conductors, mantle forming minerals

1 INTRODUCTION

The last ten years have seen an enormous growth in the application of modelling techniques to problems in solid state chemistry and materials science. In this article we aim to summarise the main methodologies used in contemporary work and to indicate the scope of the field by taking a number of applications from our recent studies. Each of these applications are of industrial importance: zeolites are important catalytic materials widely used in the petrochemicals industry, high T_c superconductors are likely to have a major impact on the electronics industry, and superionic conductors are being used in the design of highly efficient batteries. In introducing the field, we will point to some of the areas where modelling methods have made a notable contribution, which include the following:

(i) *Studies of Catalysis* especially with oxide and aluminosilicate catalysts. Modelling techniques have been applied to the study of the substrate, to the interaction of the substrate with the sorbate and to the reaction pathways of sorbed molecules. Applications of all three types of calculations to zeolite catalysts will be discussed in section (3.1)

(ii) *Solid Electrolytes*, where work over the last ten years using a range of simulation methods has been of great value in studying the structure and stability of ionically conducting solids and in elucidating diffusion mechanisms in materials such as β-Al_2O_3, Li_3N, AgI and CaF_2 (see review in reference [1]). In Section (3.3) we shall describe a recent example of the use of the molecular dynamics technique in elucidating ionic migration mechanisms in the fluoride ion conductor $RbBiF_4$.

(iii) *Ceramic Materials*, whose commercial and technological importance is growing

rapidly. The properties of the materials are commonly dominated by defects, impurities and by the behaviour of grain boundaries. Modelling methods have made substantial contributions in all these areas, especially to materials such as MgO, ZrO_2 and Al_2O_3; and in section (3.2) we will describe the results of recent simulation studies of ceramic superconductors.

(iv) *Nuclear Ceramics*, this special class of ceramic materials includes UO_2 and the mixed oxide U/PuO_2. Calculations [2] have played a vital role in understanding defect and electronic properties of these materials for which experimental study is difficult. Recent work has focussed on the behaviour of fission products where simulation methods provide one of the few ways of obtaining reliable information.

(v) *Modelling of Dense Silicates*, where the primary motivation is the understanding of geophysical materials especially under extreme conditions of high temperature and pressure. Again, modelling methods, given that they have sufficient accuracy and reliability, provide one of the most effective ways of studying such materials, as will be discussed in greater detail in section (3.4).

(iv) *Photographic, Electro-optic and Laser Host Materials* where we are concerned with 'traditional' photographic materials, principally AgCl and AgBr, and with electro-optics (for example, $LiNbO_3$ and laser materials, e.g. the garnets and the novel β''-Al_2O_3 class of materials). The behaviour of these materials is again critically dependent on defects and impurities; radiation damage processes are also clearly of importance. Simulations have proved to be of value in studying all these problems

(vii) *Non-Stoichiometric Transition Metal Oxides.* Defective non-stoichiometric materials such as $Fe_{1-x}O$ and TiO_{2-x} continue to attract attention because of interest in their complex defect structures and because of their industrial importance in e.g. oxide films. Calculations undertaken over several years are now established as one of the most effective ways of unravelling the structural complexities of the disorder in the solids, and of understanding the relationship between their defect structures and transport properties.

(viii) *Glasses.* Structural models of glass may be generated by quenched molecular dynamics techniques, and several applications of such studies have been reported. The paper by Vessal *et al.* in these proceedings describes a recent application which has looked very critically at questions relating to interatomic potentials.

Applications to *surfaces* are considered in this volume in separate papers by Parker and by Mackrodt. We continue our account with a brief summary of the main methodologies currently used in simulating the bulk properties of materials.

2 METHODOLOGY

The techniques used in solid state simulations are described in detail in several papers and reviews [1, 3, 4] and our account here will be brief. The principal methods used are as follows:-

2.1 Energy Minimisation

(a) Perfect Lattice Techniques

Lattice energies may now be readily calculated for large complex unit cells by standard simulation techniques (including the use of the Ewald procedure for the

Coulomb sums). When coupled with efficient minimisation procedures (based where possible on Newton-Raphson methods) the minimum energy crystal structure may be calculated. Such methods are now routine in crystal structure modelling. We should also note that with knowledge of the first and second derivatives of the lattice energy with respect to atom coordinates, crystal properties such as elastic and dielectric constants may be calculated as may phonon dispersion curves. Several studies have shown that where good interatomic potentials are available, accurate properties may be calculated.

All energy minimisation procedures have inherent limitations, principally the neglect of dynamical effects, the need for a 'starting point' in the minimisation procedure, and the possibility of local minima. The methods are, however, widely and routinely applicable in solid state chemistry and several automated computer codes, e.g. METAPOCS [5, 6] THBREL [7] and WMIN are available for such calculations.

(b) Defect Lattice Methods

Calculations of defect and impurity energies have been one of the most successful areas of application of simulation studies in solid state chemistry and physics. The basic methodology essentially involves an energy minimisation (or more accurately, force balance) calculation on an inner region of typically 100–500 atoms surrounding the defect, with the polarisation of the more distant region of the crystal being calculated by quasi-continuum methods. A detailed discussion of the methodology is given in reference [4]. A number of computer codes are again available, following the pioneering development of the HADES code by Norgett [8]; the most recent and comprehensive is the CASCADE program developed by Leslie [9].

2.2 Free Energy Minimisation

Using internal energy alone as a criterion for equilibrium is, of course, an approximation, which becomes increasingly inadequate at higher temperatures. Crystal free energies may, however, be calculated given knowledge of the phonon dispersion curves which enable us to calculate the perfect lattice entropy.

Using such methods phase transitions and lattice expansion may be calculated as will be discussed in section (3.4). To date, all such methods have employed the quasi-harmonic approximation in which the harmonic approximation is made for the lattice parameter appropriate to the given temperature.

Defect entropies may also be calculated by determining the perturbation of the lattice vibrations of a region of crystal surrounding the defect. Considerable success has been enjoyed in recent years by Harding, Gillan, Jacobs, Stoneham using such techniques [10, 11, 12]. It is now possible to calculate with considerable accuracy the free energies of formation of defects as a function of temperature. Recent work is given in reference [2].

2.3 Molecular Dynamics Methods

M.D. techniques are becoming used increasingly in solid state chemistry, with applications to (i) studies of ionic mobility (ii) modelling of phase transitions and (iii) simulations of glasses, being most significant in recent years. Standard NVE techniques have been extensively applied, but constant pressure and temperature techniques are also now employed. In application to polar solids the following technical

features of the calculations should be noted:

(i) The use of the Ewald technique for handling the Coulomb summations.

(ii) The generally accepted practice of omitting any effects due to electronic polarisability due to the computational expense consequent upon their inclusion. This may cause serious problems in simulating defect dependent phenomena where polarisation effects are known to be important.

Applications of MD to the study of ion transport are reported in section (3.3); these calculations were performed using the FUNGUS program which is a general package for MD simulations of ionic materials.

2.4 Monte Carlo Techniques

M.C. methods have had limited application to industrially important solids. The most promising areas of application concern first studies of the distribution of molecules in complex sorbants, where, there has been important recent work by Cheetham and coworkers; and secondly, studies of ion transport in heavily disordered materials where MC methods are particularly suited for undertaking the necessary statistical sampling of multi-jump processes. An application to oxygen diffusion in the technologically important Y/CeO_2 material is reported in reference [13].

3 APPLICATIONS

The applications included are taken from our own recent work and have been chosen so as to emphasise the complexity of the phenomena which can now be studied using simulation methods.

3.1 Zeolites

(a) Lattice Energy and Free Energy Minimisation Studies of Zeolites

The lattice energy minimisation technique has already been described in Section 2. It is only necessary to add here that in calculating energy minima, atom positions only may be varied, resulting in a constant volume result, or in addition, unit cell parameters may also be varied, leading to a constant pressure result.

The aim of this work has been first to establish whether lattice energy minimisation techniques reproduce known crystal structures of zeolites, and then to go on to use the technique predictively. Predictions can be made of relative stabilities and structures of hypothetical zeolites.

Na^+ zeolite A, whose structure is known accurately from experiment, was chosen to test the simulation method. A range of potential models were used, differing mainly in whether the oxygen ions were assumed to be rigid or polarisable. In the latter case the shell model [14] was used. In each case, the experimental structure was used as the starting structure, and minimised to constant volume. A comparison of calculated and experimental bond angles and bond lengths was then made, and in general, good agreement was obtained. Full details are given elsewhere [15] but the following general conclusions were reached:

(i) all potentials reproduce the structure to broadly the same accuracy

(ii) in general, very good agreement was obtained, except that the Si–O bond lengths were slightly underestimated in all cases,

(iii) the potentials to describe the zeolite framework were transferred from α-quartz. It is encouraging that such good agreement is obtained with potentials transferred from other sources.

Having established that lattice energy minimisation is capable of giving good agreement with experimental structures, it is possible to use the technique to make predictions about stability and structure.

To this end, lattice energies have been calculated for a range of zeolites. Table 1 lists these, and it is noted that silicalite is the most stable, which is borne out from synthesis experiments.

Recently, preliminary calculations have been carried out to obtain the entropies of these zeolites. The aim has been to establish whether these affect the relative stabilities calculated on the basis of lattice energies. It appears from these calculations that entropy contributions to the relative stabilities are very small and do not affect the calculated trends. Further work on this topic is in progress. Details of the application of this technique to silicate minerals are given in section 3.4.

(b) Quantum Mechanical Calculations on Zeolites: the Study of Methanol Adsorption in ZSM-5

The experimental study of adsorption of hydrocarbons in zeolites with a complicated pore system is an ideal topic for the application of computer simulation methods. Here, the application of modelling techniques to the study of the adsorption of methanol in ZSM-5 is considered. The ZSM-5 zeolite framework consists of cavities formed by the intersection of straight and sinusoidal pores of diameter $\sim$ 5Å running perpendicular to each other. This particular pore system makes ZSM-5 a suitable catalyst for the conversion of methanol to hydrocarbons in the gasoline range.

The ZSM-5 zeolite is modelled using the Born model. The H^+ ion is present to compensate for the charge imbalance created by Al^{3+} substituting for Si^{4+}. The proton is bonded to an O^{2-} ion bridging Si^{4+} and Al^{3+} ions. The structure used was that reported from X-ray diffraction studies, but then energy minimised to constant volume (see 3.1(a)). The resulting displacements are small. The methanol molecule is placed at the centre of the cavity in different orientations, and energy minimisation calculations were carried out to obtain the minimum energy configuration. Two distinct adsorption sites were predicted for the methanol molecule for both the siliceous framework and the aluminium substituted framework. The methanol molecule moves towards the Bronsted acid site. The calculated adsorption energies for both configurations are of the order of 0.5–1.0 eV. The calculated geometries should

Table 1 Lattice Energies for Siliceous Zeolites (rigid ion potentials; minimisations to constant pressure).

	lattice energy/SiO_2(eV)
zeolite A	−123.66
faujasite	−123.48
mordenite	−123.80
silicalite	−123.89
α quartz	−123.90

be reasonable "starting points" for quantum mechanical geometry optimisation calculations.

The quantum mechanical calculations were carried out using *ab initio* methods using both minimal (STO-3G) and extended (SV-3-21G) basis sets. The zeolite-methanol adsorption complex is represented by a cluster [HSi_2AlO_{10}:CH_3OH] containing 20 atoms. The methanol molecule and the nearest framework atoms of zeolite in a geometry predicted by lattice energy calculations were treated quantum chemically. This quantum chemical cluster was embedded in a point charge cluster containing 82 ions in order to simulate the long range forces. The point charge cluster used in the present study is the same as reported in our earlier studies of hydroxyl groups in ZSM-5.

The geometry of the clusters representing the adsorption complex, the zeolite framework and the methanol molecule was optimised to yield the minimum energy configuration. The values of the adsorption energy were calculated as:

$$\Delta H_{ads} = [T.E_{(HSi_2Al0_{10}:CH_3OH)}] - [T.E_{\cdot HSi_2Al0_{10}} + T.E_{CH_3OH}]$$

where T.E is total energy. These calculations were performed for both configurations predicted by lattice energy minimisation procedures. One of these configurations proved to be a weak adsporption with little distortion in the geometry of the complex. The calculation of the bond energy showed no tendency for cleavage of any bonds in the methanol molecule. However, in the other configuration, methanol interacted strongly with the framework atoms and a considerable distortion of the geometry of the adsorption complex was observed in the final minimum energy configuration. One of the hydrogens of the methyl group in the methanol is abstracted by the zeolite and a [CH_3OH] species is formed. There appears to be no activation energy barrier to the

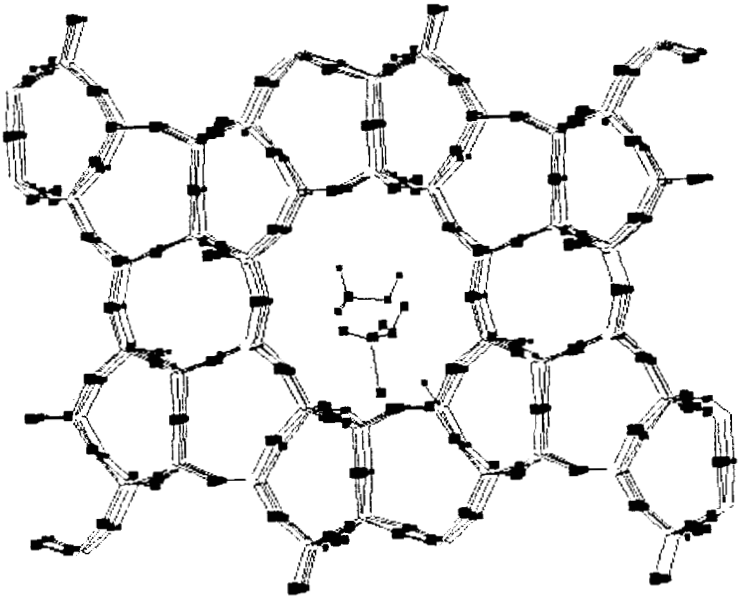

Figure 1 Initial and Final Positions of the Methanol Molecule in the Zeolite Lattice. (See colour plate I.)

formation of this species. The initial position of the methanol molecule in the quantum mechanical calculation, and the final position, showing the formation of the $[CH_2OH]$ species, are shown in Figure 1.

Thus by a combination of modelling and quantum mechanical calculations, the sorption site and primary reaction of methanol in ZSM-5 have been predicted.

3.2 Simulation Studies of High T_c Superconducting Oxides

In this section we report recent studies of the high T_c superconducting oxide La_2CuO_4. Most current theories of superconductivity involve pairing of charge carriers with opposite spins [16]; the resulting bipolaron species will thus have zero momentum and cannot be affected by collisions with the lattice. Hence resistance free conduction is possible. It is obvious, therefore, that an understanding of the nature of the charge carriers, how and under what conditions they are formed and the mechanism of bipolaron formation is essential. Static simulation techniques are now sufficiently advanced that they can be usefully employed to study all these problems.

The primary requirement for the simulation study are the parameters in the potential energy function which describes the total crystal potential in terms of a sum of pairwise and three-body interactions. We derived these parameters by a process of empirical fitting to the structure and properties of the binary oxide precursors of the $La_{2-x}(Sr, Ba)_xCuO_4$ system. Such a procedure has been successfully employed in the study of other complex materials [6], and has two main advantages. First, extensive crystal data is available for the binary oxides. Such data is not yet available for the

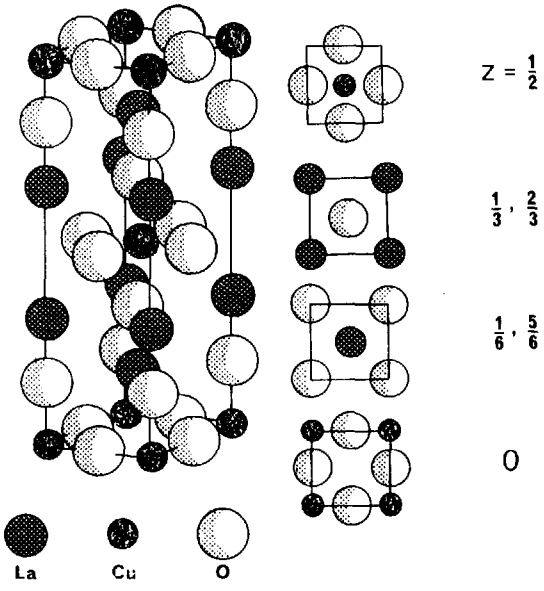

Figure 2 The Structure of La_2CuO_4 (after Yu *et al.* [37]).

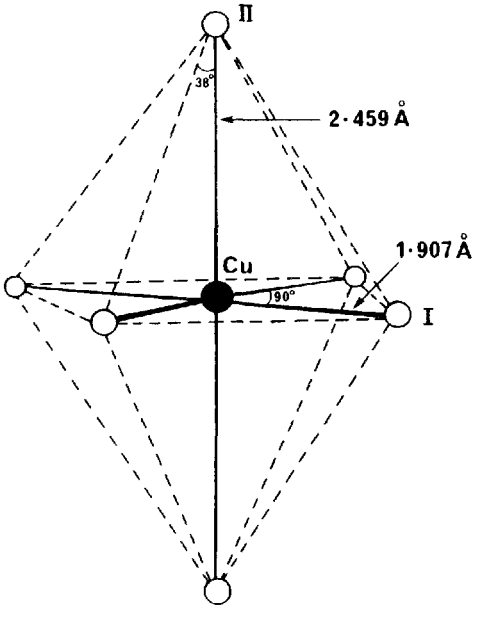

Figure 3 Axially distorted CuO_6 unit in La_2CuO_4. Angles around which bond-bending potentials operate are shown (after Grande *et al.* [18]).

ternary and quaternary systems we wish to study, therefore, it is not possible to fit the parameters directly. Secondly, transferring parameters from binary oxides will permit a systematic study of other superconducting oxides. It is obviously desirable to use the same parameters for the Cu . . O interaction in the La_2CuO_4 system and the $Ba_2YCu_3O_7$ system.

We found it necessary to include three-body interactions to accurately reproduce the structure of CuO. We use a bond-bending model for this type of interaction which adds a term E to the potential energy function [17] of the form

$$E = \tfrac{1}{2}k_B(\theta - \theta_0)^2$$

In the above expression k_B is the bond force constant and θ_0 the equilibrium bond angle. It has the effect of constraining specified bond angles to have the observed value, θ_0. CuO consists of elongated CuO_6 octahedra, and the higher order terms are necessary to model this distortion. The same elongation of CuO_6 octahedra is found in La_2CuO_4, the structure of which is shown in Figure 2. The bond angles about which bond-bending interactions operate are shown in Figure 3. The potential model we obtain from the procedure described above yields an equilibrium structure for La_2CuO_4 which is very close to the observed orthorhombic form [18]. The values of the parameters in the model are reported elsewhere [19].

A further, and exacting, test of the potential model is to calculate the phonon dispersion curves for the material. We have done so for a series of wave vectors (see

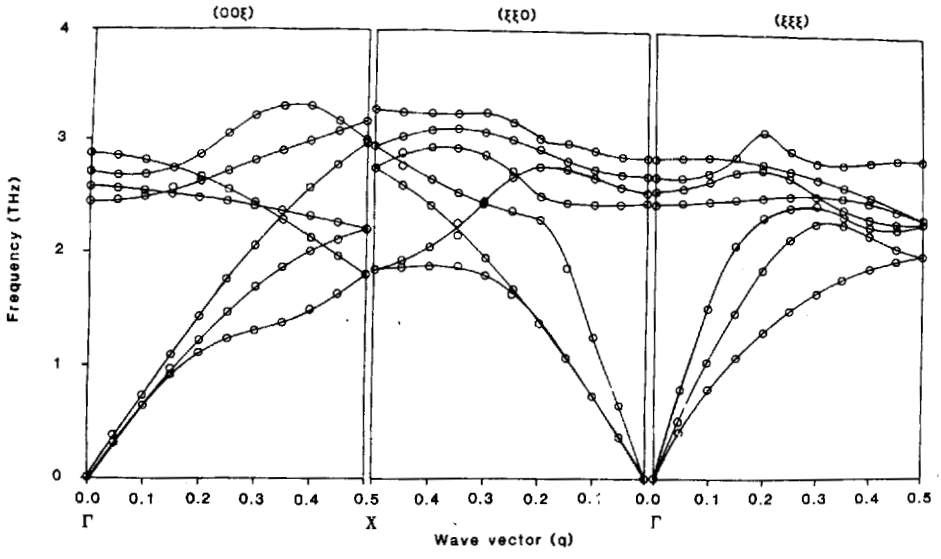

Figure 4 Calculated phonon dispersion curves for La_2CuO_4; (OOξ), (ξ ξ O) and ξ ξ ξ) directions.

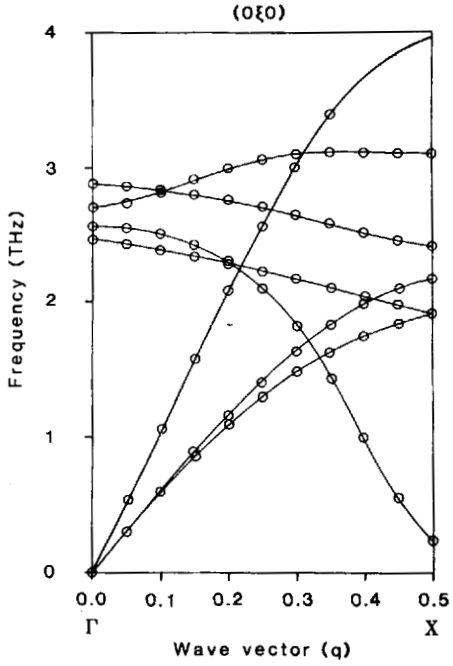

Figure 5 Calculated phonon dispersion curves for La_2CuO_4 in the (O ξ O) direction.

Figure 4) and found that all branches are positive; which further supports the quality of our model. Moreover, for the (0, ξ, O) direction we find a softening of one of the low lying optical branches (Figure 5). This agrees remarkably well with the observed behaviour [20]. We note that the axes in the phonon frequency plot, given by Birgeneau *et al.* [20], are labelled with respect to the tetragonal cell, whereas ours refer to the orthorhombic. Phonon mode softening has been the subject of considerable speculation, as it is thought to be connected with the favourable interaction between phonons and charge carriers in superconductors.

We have studied defect and valence states in La_2CuO_4 using the CASCADE code [19]. We treat the charge carrier as a small polaron because we are using a fully ionic model, i.e. we alter ionic charges by integral amounts in order to create a hole or electron state. Table 2(a) contains the formation energies of electronic defects. We have reported values calculated for both thermal and optical processes. In the latter calculation only the ion shells (within the shell model [14]) are allowed to relax to their equlibrium positions in response to defect formation. In the thermal calculation both cores and shells are allowed to relax. The polarisation energy we obtain from the optical calculation may be equated with the purely *electronic* polarisation surrounding the defect. The difference between the results of the optical and thermal calculations gives the *displacement* polarisation energy. It is evident from table 2(a) that both electronic and displacement polarisation energies are large. The magnitudes indicate

Table 2(a) Formation energies of isolated defects and substitutionals

Species	*Energy (eV)*		*Electronic polarisation energy (eV)*	*Displacement polarisation energy (eV)*
	thermal	*optical*		
Cu^{+}	21.68	24.37	3.38	2.69
Cu^{3+}	33.92	−31.22	3.07	2.70
O^{-} (1)	14.19	17.19	2.03	3.00
O (2)	14.75	18.22	1.82	3.47
$V_O^{\cdot\cdot}$ (1)	15.93			
$V_O^{\cdot\cdot}$ (2)	17.73			
Ba'_{La}	24.09			
Sr'_{La}	21.38			

(1) equatorial oxygen site
(2) axial oxygen site

Table 2(b) Atomic and Lattice energies. Key: I_2 and I_3 are the second and third ionisation potentials of copper; E_1 and E_2 are the first and second electron affinities of oxygen; D_e is the dissociation energy of an O_2 molecule.

Term	*Energy (eV)*
I_2	20.39
I_3	36.83
E_1	1.47
E_2	−8.75
D_e	5.16
$E_{Lat}(BaO)$	−31.25
$E_{Lat}(SrO)$	−33.42
$E_{Lat}(La_2O_3)$	−126.12

the strength of the polaron lattice interaction in this oxide. We may combine the results of the CASCADE calculations with the free ion ionization potentials and electron affinities. For example, the value we calculate for Cu^{3+} formation with CASCADE represents the energy required to remove a Cu^{2+} ion to infinity, replace it with a Cu^{3+} ion from infinity, and relax the surrounding lattice. Thus it is necessary to add the free ion ionization energy of Cu^{2+} to obtain the total formation energy of Cu^{3+} in La_2CuO_4. In table 2(b), we report the free ion terms, and in Table 3 we report the hole state formation energies. Our calculations suggest that the hole state will be Cu^{3+} in nature, rather than O^-.

The superconducting phases generally contain up to 15% Ba and Sr substituted for La. A possible charge compensating mechanism for such a substitution is the formation of oxygen vacancies. These may form either at equatorial (0(1)) or axial (0(2)) sites. From Table 2(a) we note the important result that oxygen vacancy formation will occur at the equatorial site. We may combine our results for oxygen vacancy formation with our calculated substitution energies of Ba and Sr at the La site (also reported in Table 2(a)), and with the appropriate calculated lattice energies given in Table 2(b). We then obtain the solution energies of BaO and SrO in La_2CuO_4. The results are given in Table 3. For BaO the value is small and positive and for SrO small and negative. Both these results accord with the experimental observation that these oxides readily dissolve in La_2CuO_4 to yield the superconducting phases.

We may also investigate the stability of oxygen vacancies with respect to oxidation of the doped material. The result of this calculation is shown in Table 3. The process is exothermic which suggests that the doped material will readily oxidise to form Cu^{3+} ions; i.e. creating charge carriers. Another process which may create charge carriers is copper disproportionation. We have investigated this mechanism and found it to be highly unfavourable both thermally and optically (see Table 3).

Finally in this section we discuss our calculations on bipolaron stability in La_2CuO_4. We mentioned earlier that such entities are often claimed to be involved in superconductivity. The proposed pairing mechanism is that Coulomb repulsion is overcome by the favourable polarisation response of the surrounding lattice. Static simulation provides a unique and straightforward way of studying bipolaron stability. We have calculated the formation and binding energies of different configurations of bipolarons [19]. The results for two configurations are reported in Table 4. The first involves Cu^{3+} ions on nearst neighbour copper sites in the same Cu–O plane (configuration A in Table 4), and second has the Cu^{3+} ions located at nearest neighbour copper sites in adjacent layers (configuration B in Table 4). We note first that neither appear to be bound; i.e. the binding energies are positive. However, it is possible that

Table 3 Energies of hole formation, charge transfer, solution and oxidation processes.

Process	*Energy (eV)*	
Total formation energy for Cu^{3+} ion	thermal	2.91
	optical	5.61
Total formation energy for O^- ion	thermal	5.44
	optical	8.44
$2Cu^{2+} \rightarrow Cu^{+} + Cu^{3+}$	thermal	4.20
	optical	9.59
$BaO \rightarrow Ba'_{La} + 1/2V_O^{\cdot\cdot} + 1/2La_2O_3$	thermal	0.25
$SrO \rightarrow Sr'_{La} + 1/2V_O^{\cdot\cdot} + 1/2La_2O_3$	thermal	−0.29
$V_O^{\cdot\cdot} + 1/2O_2 \rightarrow O_O^{x} + 2Cu^{\cdot}_{Cu}$	thermal	−0.25

Table 4 Energies of bipolaron formation.

Bipolaron Configuration	*Energy (eV)*	*Binding energy (eV)*	*Polarisation energy (eV)*	*Change in Polarisation energy (eV)*
A Intra-layer	thermal −67.38	0.46	15.51	3.97
	optical −60.37	2.07	8.51	2.37
B Inter-layer	thermal −67.80	0.04	14.18	2.64
	optical −61.52	0.92	7.91	1.77

the effective Coulomb repulsion is less than the Coulomb repulsion term in our model, due to screening effects. Furthermore, we note that the polarisation energies of bipolarons are greater than the sum of the polarisation energies of two isolated polarons. This suggests that lattice polarisation *is* a possible coupling mechanism for polarons in La_2CuO_4. It may well be that an inclusion of screening would yield favourable binding energies for bipolarons, or that there are additional coupling mechanisms not fully incorporated in our model [36].

We have shown in this section that static simulation methods are a powerful tool for probing the fundamental lattice dynamical and defect processes in La_2CuO_4. We are currently extending the work to include a treatment of screening effects in bipolaron formation, and we are also studying the $YBa_2Cu_3O_{7-x}$ system.

3.3 Molecular Dynamics Studies of $Rb_{1-x}Bi_xF_{1+2x}$

γ-$RbBiF_4$ belongs to a class of materials known as superionic conductors, which were referred to in the introduction. These are defined as crystalline solids which show ionic conductivities typical of those found for molten salts (i.e. σ $10^{-1}\Omega^{-1}cm^{-1}$). Non-conducting salts such as NaCl exhibit conductivities of 10^{-12} – $10^{-16}\Omega^{-1}cm^{-1}$ at room temperature. There are extensive applications for superionic conductors including use as battery electrolytes, high temperature thermometers, gas sensors and fuel cells. Other examples of superionic conductors include layer structured materials β–Al_2O_3 and LiN_3, fluorite-oxide solid solutions such as ZrO_2/CaO and CeO/Y_2O_3, and the high temperature phases of certain halides such as AgI.

γ-$RbBiF_4$ adopts the fluorite structure (Figure 6). Neutron scattering data suggests that the cations are randomly distributed over the available cation sites [21]. Supplementary fluorine ions may be accommodated to form solid solutions of the formula $Rb_{1-x}Bi_xF_{1+2x}$ as well as an ordered $RbBi_3F_{10}$ (x = 0.75) compund. This consists of alternate $[RbBi_3F_8]^{2+}$ and $[RbBi_3F_{12}]^{2-}$ groups. The F_8 motifs are cubic whilst the F_{12} ones form a sub-octahedral cluster (Figure 7). As x increases from 0.5 to 0.75, the ionic conductivity steadily decreases [21] (Figure 8).

The high levels of disorder within these materials make it difficult to obtain detailed information on them from experiment. We have used the MD technique to yield valuable information on their structure and transport properties. We have collected data for three compositions, x = 0.5, 0.6, and 0.75 at three temperatures, 80K, 473K and 700K. The interatomic potentials were taken from those of the appropriate binary fluorides [22, 23]. A time-step of 5×10^{-15} seconds was used. Each simulation was equilibrated for 1000 time-steps and then run for a further 3000 time-steps. The

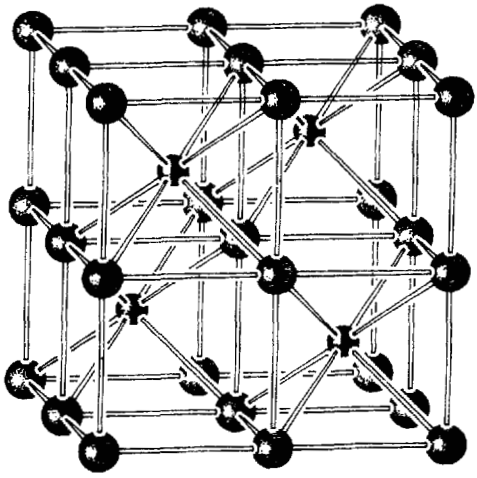

Figure 6 The fluorite structure (cations occupy cube centres). (See colour plate II.)

work was performed on the CRAY-1S computer at the university of London Computer Centre using the program FUNGUS [24].

The input structures for the three compositions were as follows:-

(i) $x = 0.5$ The particles were assigned the co-ordinates of the fluorite structure. The cations were randomly distrbuted over the available cation sites. A large simulation box was used (768 ions) to accommodate this feature.

(ii) $x = 0.6$ Two models were used: (a) The fluorite structure with cations randomly distributed over the available cation sites. The additional fluorine ions were placed at interstitial sites. (b) As Model (ii) (a), but with two cubo-octahedral clusters per simulation box (thus introducing some cation ordering).

(iii) $x = 0.75$ Alternate $[RbBi_3F_8]^{2+}$ and $[RbBi_3F_{12}]^{2-}$ motifs, with a fully ordered cation sublattice.

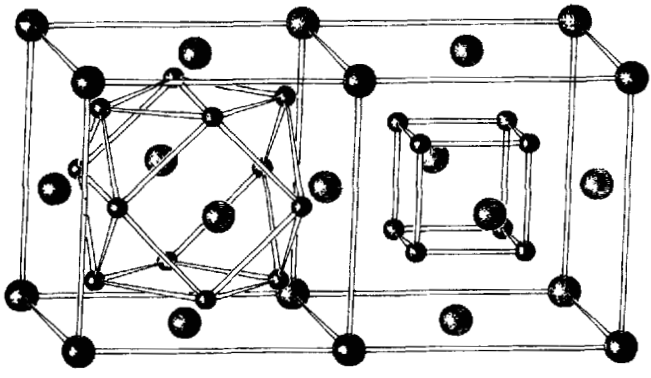

Figure 7 The ordered anion-excess structure adopted by $RbBi_3F_{10}$. The Rb^+ ions occupy cube corners, and the Bi^{3+} ions occupy face centres. The remaining ions are F^-. (See colour plate III.)

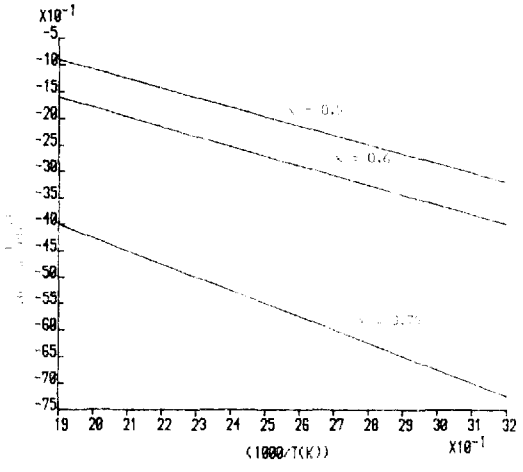

Figure 8 Temperature dependence of the conductivity for $Rb_{1-x}Bi_xF_{1+2x}$.

The results of the simulations are now discussed.

x = 0.5

In Figure 9 we present the calculated radial distribution functions (rdfs) for the two cations at 80K. These reproduce qualitatively all the features of the experimental EXAFS Fourier transforms (Figure 10) for the two cation edges (Fourier transforming EXAFS data produces an approximate radial distribution function) [25], specifically:-

(1) Both radial distribution functions contain only one well-defined peak i.e. the level of disorder in the material is modelled satisfactorily.

(2) The peak in the Rb rdf is broader than the peak in the Bi rdf. i.e. the static disorder in the Rb–F coordination shell is greater than the Bi–F one.

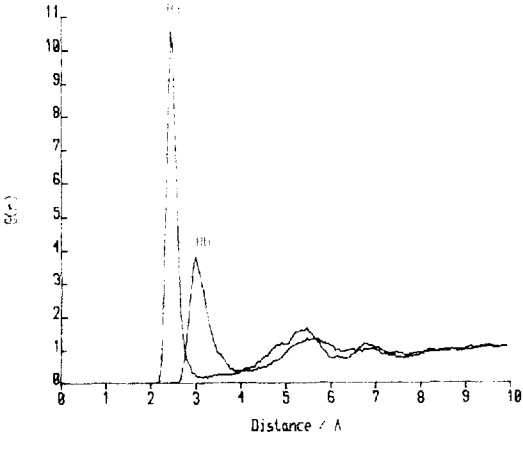

Figure 9 Calculated radial distribution functions for the equilibrated MD structure for $RbBiF_4$ at 80 K.

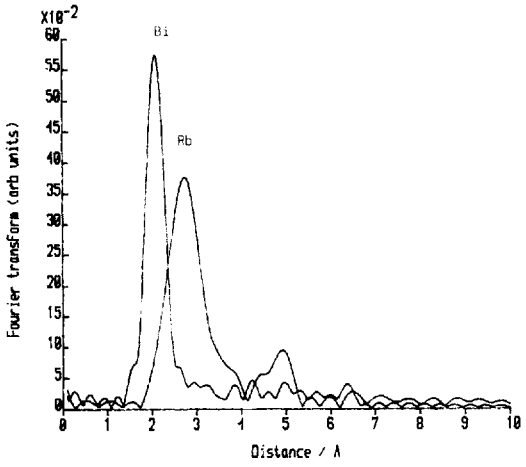

Figure 10 EXAFS Fourier transforms at 80 K.

(3) The peak in the Rb rdf is at ~ 0.5 Å higher than the peak in the Bi rdf i.e. the Rb–F bond length is 0.5 Å more than the Bi–F bond length.

This agreement suggests that the equilibrium structure of the simulation is in good agreement with the actual structure. Analysis of the structure generated shows that whilst the cations retain their original coordinates, the anions form a complex, grossly distorted 'cubic' structure. The local environment of each cation depends upon the other cations in its coordination shell. The occupancy of the interstitial site is high (~ 12% at 80K). This is in good agreement with neutron diffraction studies [26]. Analysis of the coordinates of diffusing ions reveals that these interstitial ions play a key role in the diffusion mechanism, with ions hopping from 'lattice site' to 'lattice site' via the interstitial position (Figure 11). The motion of the ions is highly correlated (Figure 12), which is almost certainly one of the factors promoting high F^- ion conductivity in these materials.

X = 0.6

For the model incorporating additional fluorine ions at interstitial sites, with no cation ordering, we observe an increase in the rate of fluorine ion diffusion over the

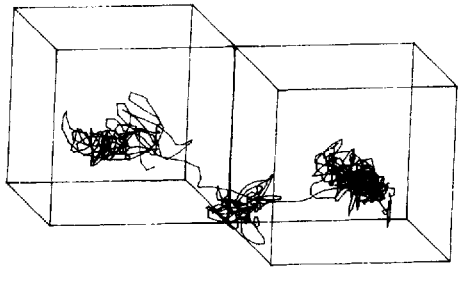

Figure 11 A F^- ion diffusing through $RbBiF_4$ via a non-collinear interstitialcy mechanism.

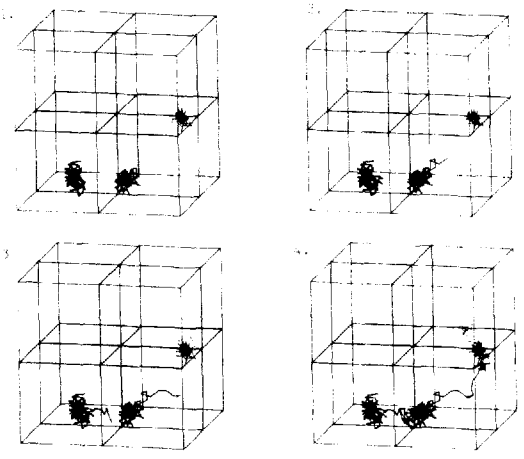

Figure 12 F^- migration is via a concerted mechanism. The figure shows four 'snapshots' of this mechanism. In the colour version, each ion trajectory has a different colour. (See colour plate IV.)

$x = 0.5$ simulation (Figure 13). This disagrees with the experimentally observed result. Incorporating just two clusters per simulation box, however, reduces the rate of fluorine ion diffusion to below that of the $x = 0.5$ material. These results suggest that clusters form as x increases from 0.5. Our experimental EXAFS work supports this.

$x = 0.75$

The input structure is extremely stable, with no occupancy of interstitial sites taken up. No diffusion is observed during the course of the simulation (Figure 14).

A random distribution of cations leads to uneven forces upon the F^- ions within $\gamma RbBiF_4$. This distorts the anion sublattice, and forces many ions into the interstitial

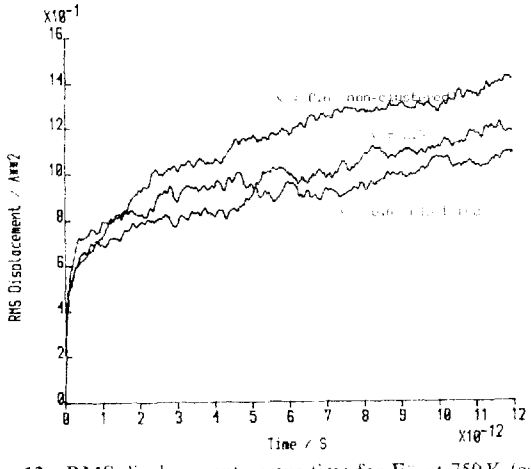

Figure 13 RMS displacement versus time for F^- at 750 K (case 1).

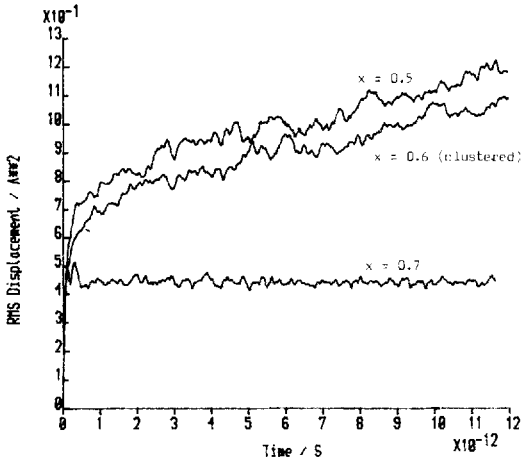

Figure 14 RMS displacement versus time for F^- at 750 K (case 2).

sites, even at low temperatures. These interstitials facilitate diffusion via a non-collinear interstitialcy mechanism, and lead to the superionic behaviour of the material.

As we increase x, cation ordering occurs which leads to the formation of clusters, as found in the x = 0.75 material. Within these clusters, fluorine ions are 'trapped' within the motifs and hence the concentration of interstitials diminishes, causing a reduction in the conductivity.

On the basis of this work, an interesting experiment would be to attempt to synthesise x > 0.5 materials, trying to prevent clusters from forming, possibly by the use of rapid quenching techniques. These, we postulate, would have higher conductivities than the 0.5 material.

3.4 Free Energy Minimisation of Minerals

In this section we briefly describe the technique for modelling the thermodynamic properties and phase relations of silicate minerals. Of particular interest are the magnesium silicates which dominate the Earth's Mantle. Seismic wave studies have revealed that the mantle is layered with major discontinuities at about 400 and 700 Km which partition the mantle into three 'zones,' namely, the Upper Mantle, Transition Zone and Lower Mantle. Currently, the 'zones' are believed to be comprised of three distinct phases of magnesium silicate. Evidence for this comes from seismic and meteorite studies and more recently from diamond anvil experiments which are now able to reach the required temperatures and pressures, although because of the extreme conditions it is not always possible to obtain highly accurate quantitative data. Computer simulation does not suffer from these problems, therefore this approach may provide a powerful technique for modelling the high temperature and pressure phenomena. We therefore investigated the stability of the four magnesium phases which are thought to exist in the mantle. These are, olivine, beta-phase, spinel and perovskite, where the first three phases are associated with the Upper Mantle and Transition Zone, while the latter is believed to coexist with MgO in the Lower Mantle. The ambient stable phase has the olivine structure and stoichio-

metry Mg_2SiO_4. This is characterised by a hexagonal close-packed oxygen sublattice and isolated SiO_4^{4-} tetrahedra. At higher pressures and temperatures the beta-phase is formed, which has the same stoichiometry but has cubic close-packed oxygens and $Si_2O_7^{6-}$ groups, consisting of pairs of tetrahedra. As the pressure is further increased spinel is formed and is structurally similar to beta-phase except the SiO_4^{4-} tetrahedra are isolated from each other. The perovskite structured magnesium silicate is quite distinct as the silicon is coordinated to six oxygens and magnesium to eight.

Previous work [27–29] has shown that these materials can be modelled with a high degree of precision. An empirically derived potential model was used where the parameters describing the short range interactions were transferred from the component oxide. An additional term was added for the beta-phase, namely a Si–O–Si bond bending term to model the $Si_2O_7^{6-}$ group. In general the crystal properties gave good agreement with experiment; the major differences were in the elasticity data, probably because we used a central force potential for magnesium oxide which may not be appropriate given the large Cauchi violations. Central force potentials predict that the elastic constants C_{12} and C_{44} are equal; experimentally they are found to differ. This is known as the Cauchi violation.

The approach used to calculate crystal properties at elevated temperatures uses energy minimisation. But unlike earlier work the *free-energy* is minimised by adjusting the cell dimensions until the free-energy achieves a minimum value. Throughout the simulation the atom positions are modified so the atoms experience zero mechanical strain. The free-energy is calculated from the lattice energy and vibrational free-energy. The latter is obtained from the phonon density of states. This method makes the assumption that the lattice vibrations are harmonic which may fail at high temperatures. In addition, to generate a complete phonon density of states, over a thousand points in reciprocal space need to be considered (the vibrational frequencies can vary markedly with position in reciprocal space) – which is too computationally expensive. Therefore we use sampling methods [30, 31] Our work on olivine [28, 29] suggests that the free-energy can be obtained from as little as eight points in reciprocal space, to the accuracy we require. Thus to calculate the solid state phase diagram we need only calculate the minimum free-energy of each phase over a range of tem-

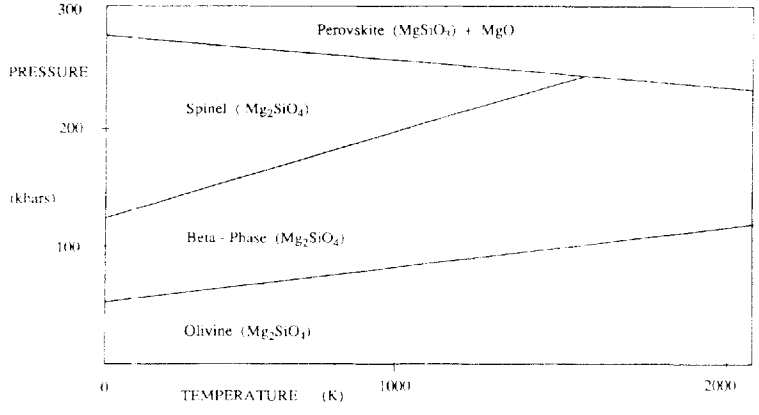

Figure 15 The calculated Phase Diagram of Mg_2SiO_4.

Table 5 *Phase Relations*, $P_T = P_0 + mT$.

	Experimental	*Calculated (this work)*
Olivine – Beta		
ref 33	98 + 0.035T	51 + 0.018T
ref 32	116 + 0.025T	
ref 34	57 + 0.058T	
Beta – Spinel		
ref 33	100 + 0.055T	113 + 0.056T
ref 32	117 + 0.048T	
ref 34	70 + 0.055T	
Spinel – Perovskite		
ref 32	273 – 0.020T	279 – 0.033T
Beta – Perovskite		
	–	237 – 0.010T

peratures and pressures. We have performed these simulations for the phases described above, and the results are given in Table 5 and Figure 15 [35].

The major features of the plot are that the olivine-beta and beta-spinel boundaries have positive grandients and show no triple point. This is in contrast to experimental work [32, 33] which give one for olivine-beta-spinel phases, but recent work [34] shows no such point, in agreement with our simulations. However, the energy differences are small $\sim$ 4–20 kJmol^{-1} compared with the lattice energies of $\sim$ 20000 kJmol^{-1} so that there is still some room for doubt. Perhaps a much more critical test for the potentials is the boundary between spinel and perovskite as there is a significant change in cation coordination between the two structures. Our simulation calculates a negative slope, ~ -0.033 kbars/T which is in remarkably good agreement with experiment [32] particularly given the large degree of uncertainty in the experiment.

In summary, atomistic simulation techniques provide a valuable technique for modelling the phase relations of solids. The major benefit will be seen when the effects of impurities, which are present in large concentrations in the mantle, on the phase stability are investigated, particularly given the difficulty in comparable experimental techniques.

Acknowledgements

We would like to thank the SERC, ICI Plc and Shell Research BV for financial support.

References

[1] C.R.A. Catlow, 'Computer Simulation Studies of Transport in Solids,' *Ann. Rev. Mater. Sci.*, **16,** 517 (1986).
[2] R.A. Jackson, A.D. Murray, J.H. Harding and C.R.A. Catlow, 'The Calculation of Defect Parameters in UO_2,' *Phil. Mag.* **53,** 27 (1986).
[3] C.R.A. Catlow and A.N. Cormack, 'Computer Modelling of Silicates,' *Int. Rev. Phys. Chem.* **6,** 227 (1987).
[4] C.R.A. Catlow and W.C. Mackrodt, eds, *Computer Simulation of Solids*, Lecture Notes in Physics no. 166, Springer-Verlag, Berlin, 1982.
[5] C.R.A. Catlow, A.N. Cormack and F. Theobald, 'Structure Prediction of Transition-Metal Oxides using Energy-Minimisation Techniques,' *Acta Cryst.*, **B40,** 195 (1984).

[6] S.C. Parker, C.R.A. Catlow and A.N. Cormack, 'Structure Prediction of Minerals using Energy-Minimisation Techniques,' *Acta Cryst.*, **B40,** 200 (1984).
[7] M. Leslie, SERC Daresbury Laboratory Report – *in preparation.*
[8] M.J. Norgett, 'A General Formulation of the Problem of Calculating the Energies of Lattice Defects in Ionic Crystals,' UKAEA Report R7650 (1974).
[9] M. Leslie, 'Program Cascade. Description of Datasets For Use in Crystal Defect Calculations,' SERC Daresbury Laboratory Report DL/SCI/TM31T (1982).
[10] M.J. Gillan and P.W.M. Jacobs, 'Entropy of a Point Defect in Ionic Crystals,' *Phys Rev B,* **28,** 759 (1983).
[11] J.H. Harding and A.M. Stoneham, 'Vibrational entropies of defects in solids,' *Phil Mag B,* **43,** 705 (1981).
[12] J.H. Harding, 'The Calculation of Free Energies of Point Defects in Ionic Crystals,' *Physica,* **131B,** 13 (1985).
[13] A.D. Murray, G.E. Murch and C.R.A. Catlow, 'A New Hybrid Scheme of Computer Simulation Based on Hades and Monte Carlo: Application to Ionic Conductivity in Y^{3+} doped CeO_2,' *Solid State Ionics,* **18 & 19,** 196 (1986).
[14] B.G. Dick and A.W. Overhauser, 'Theory of the Dielectric Constants of Alkali Halide Crystals,' *Phys. Rev.,* **112,** 90 (1958).
[15] R.A. Jackson and C.R.A. Catlow, 'Computer Simulation Studies of Zeolite Structure,' *Molecular Simulation,* **1,** 207 (1988).
[16] N.H. March and M. Parrinello, *Collective Effects in Solids and liquids,* Adam Hilger, Bristol (1982).
[17] M.J. Sanders, M. Leslie and C.R.A. Catlow, 'Interatomic Potentials for SiO_2,' J. Chem. Soc. Chem. Commun., 1271 (1984).
[18] B. von Grande, Hk. Müller-Buschbaum and M. Schweizer, 'Zur Kristallstruktur von Seltenerdmetall-loxocupraten: La_2CuO_4, Gd_2CuO_4,' *Z. Anorg. (Allg.) Chem.,* **428,** 120 (1977).
[19] M.S. Islam, M. Leslie, S.M. Tomlinson and C.R.A. Catlow, 'Computer Modelling Studies of Defects and Valence States in La_2CuO_4,' *J. Phys. C.,* **21,** L109 (1988).
[20] R.J. Birgeneau, C.Y. Chen, D.R. Gabbe, H.P. Jenssen, M. Kastner, C.J. Peters, P.J. Picone, T. Thio, T.R. Thurston, H.L. Tuller, J.D. Axe, P. Böni and G. Shirane, 'Soft-Phonon Behaviour and Transport in Single Crystal La_2CuO_4,' *Phys. Rev. Lett.,* **59,** 1329 (1987).
[21] S.F. Matar, 'Modes de conduction, defalts ponctuels et étendus dans de nouveaux fluorures et oxyfluorores de structure fluorine et derivée: Etudes expérimentales et approaches théoriques: Ph.D. thesis, University of Bordeaux, 1983.
[22] C.R.A. Catlow, K.M. Diller and M.J. Norgett, 'Ion transport and interactomic potentials in the alkaline-earth fluoride crystals,' *J. Phys. C.,* **10,** 1395 (1977).
[23] S.F. Matar, J.M. Reau and P. Hagenmuller, 'The cubo-octahedral cluster in the fluorite-type lattice: a theoretical approach,' *J. Solid State Chem.,* **52,** 114 (1984).
[24] J.R. Walker, 'Molecular Dynamics Simulations of Crystalline Ionic Materials,' in *Computer Simulation of Solids* (eds. C R.A. Catlow and W.C. Mackrodt), Lecture Notes in Physics No. 166, Springer-Verlag, Berlin. 1982
[25] E.A. Stern, D.E. Sayers and F.W. Lytle, 'Extended X-ray Absorption Fine Structure techniques III: determination of physical parameters,' *Phys. Rev. B,* **11,** 4836 (1975).
[26] J.L. Souberoux, J.M. Reau and M.J. Gillan, *Solid State Ionics* **6,** 103 (1982).
[27] S.C. Parker and G.D. Price, 'A Study of the Structures and Energetics of Magnesium Silicates,' *Physica,* **131B,** 290 (1985).
[28] G.D. Price, S.C. Parker and J. Yeomans, 'The Energetics of Polytypic Structures: A Computer Simulation of Magnesium Silicate Spinelloids,' *Acta Cryst,* **B41,** 231 (1985).
[29] G.D. Price, S.C. Parker and M. Leslie, 'The Lattice Dynamics and Thermodynamics of the Mg_2SiO_4 polymorphs,' *Phys. Chem. Minerals,* **15,** 181 (1987).
[30] G. Filippini, C.M. Gramaccioli, M. Simonetta and G.B. Suffritti, 'Lattice-Dynamical Applications to Crystallographic Problems: Consideration of Brillouin Zone Sampling,' *Acta Cryst.* **A32,** 259 (1976).
[31] D.J. Chadi and M.L. Cohen, 'Special Points in the Brillouin Zone,' *Phys. Rev. B,* **8,** 5747 (1973).
[32] T. Ashida, S. Kume and E. Ito, 'Thermodynamic Aspects of Phase Boundary among Alpha, Beta and Gamma Mg_2SiO_4,' in *High Pressure Research in Mineral Physics* (eds M. Manghnani and Y. Syono), Geographical Monograph 39, 269 (1987), American Geophysical Union, Washington.
[33] K. Suito, 'Phase Relationships of pure Mg_2SiO_4 up to 200 kbar, in *High Pressure Applications to Geophysics* (eds M. Manghnani and S. Akimoto), 255 (1977), Academic Press, New York.
[34] K. Kawada, 'The System Mg_2SiO_4 – Fe_2SiO_4 at High Pressures and Temperatures and the Earth's

Interior,' Ph.D. thesis, University of Tokyo, (1977).
[35] I.A. Marshall, S.C. Parker and G.D. Price, 'Computer Simulation of the Structure and Stability of Silicate Minerals', *Submitted to* J. Chem. Soc. Chem. Commun.
[36] C.R.A. Catlow, S.M. Tomlinson, M.S. Islam, M. Leslie, 'Hole Pairing Mechanisms in La_2CuO_4,' submitted to J. Phys. C.
[37] J. Yu, A.J. Freeman, J.-H. Xu, 'Electronically Driven Instabilities and Superconductivity in the Layered $La_{2-x}Ba_xCuO_4$ Perovskites,' *Phys. Rev. Letters*, **58,** 1035 (1987).